Supplementary Information

Pioneering dielectric materials of Sn–doped $Nb_{0.025}Ti_{0.975}O_2$ ceramics with excellent temperature and humidity stability for advanced ceramic capacitors

Yasumin Mingmuang [1], Narong Chanlek [2], Masaki Takesada [3,*], Ekaphan Swatsitang [1], & Prasit Thongbai [1,*]

[1] *Giant Dielectric and Computational Design Research Group (GD–CDR), Department of Physics, Faculty of Science, Khon Kaen University, Khon Kaen 40002, Thailand*

[2] *Synchrotron Light Research Institute (Public Organization), 111 University Avenue, Muang District, Nakhon Ratchasima 30000, Thailand*

[3] *Department of Physics, Hokkaido University, Sapporo, 060-0810, Japan*

**E–mail address:* pthongbai@kku.ac.th (P. Thongbai); mt@phys.sci.hokudai.ac.jp (M. Takesada)

Table 1 Lattice parameters, Raman shifts of E_g and A_{1g} modes, and bond lengths for 1%Sn–NTO, 2.5%Sn–NTO, and 5%Sn–NTO ceramics.

Sample condition	1%Sn–NTO	2.5%Sn–NTO	5%Sn–NTO
$a = b$ (Å)	4.605(9)	4.608(7)	4.611(9)
c (Å)	2.965(6)	2.969(2)	2.973(9)
E_g (cm^{-1})	438.7	438.0	436.5
A_{1g} (cm^{-1})	606.1	606.6	607.2
Bond length (Å)	**A** = Ta, Sn, Ti		
$\mathbf{A}_{(0,0,0)}$–$O_{(0.19480, -0.19480, 0.50000)}$	1.952(0)	1.953(0)	1.956(0)
$\mathbf{A}_{(0,0,0)}$–$O_{(0.30520, 0.30520, 0.00000)}$	1.988(0)	1.989(0)	1.991(0)
$\mathbf{A}_{(0,0,0)}$–$O_{(0.30520, -0.69480, 0.00000)}$	3.495(1)	3.497(1)	3.500(1)
$\mathbf{A}_{(0,0,0)}$–$A_{(0, 0, 1)}$	2.966(1)	2.969(1)	2.974(1)

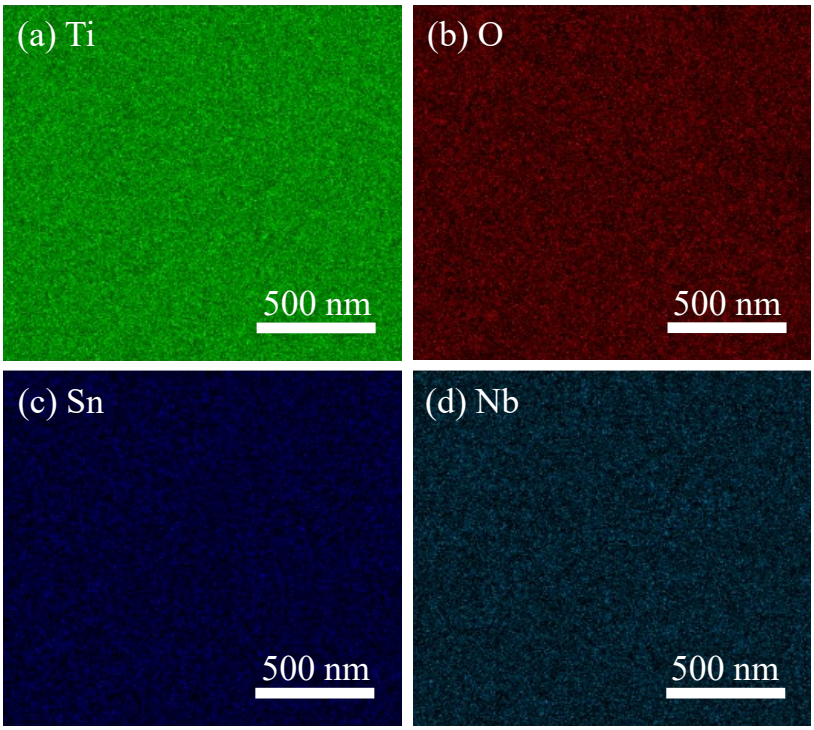

Fig. S1 SEM mapping of (a) Ti, (b) O, (c) Sn, and (d) Nb for 5%Sn–NTO ceramic.

Fig. S1 presents mapping images of all elements in 5%Sn–NTO ceramic sintered at 1200 °C for 3h. Generally, a second phase was observed in specific regions, such as grain boundaries, which were indicated by lighter areas in the elemental mapping. Notably, a homogeneous distribution of Sn, Nb, Ti, and O elements was detected along both grains and grain boundaries on the surface morphology of the 5% Sn–NTO ceramic. There was no accumulation of several phases in specific regions, indicating the absence of secondary phases. The result is similar to other works in co–doped rutile TiO_2 ceramics [1, 2].

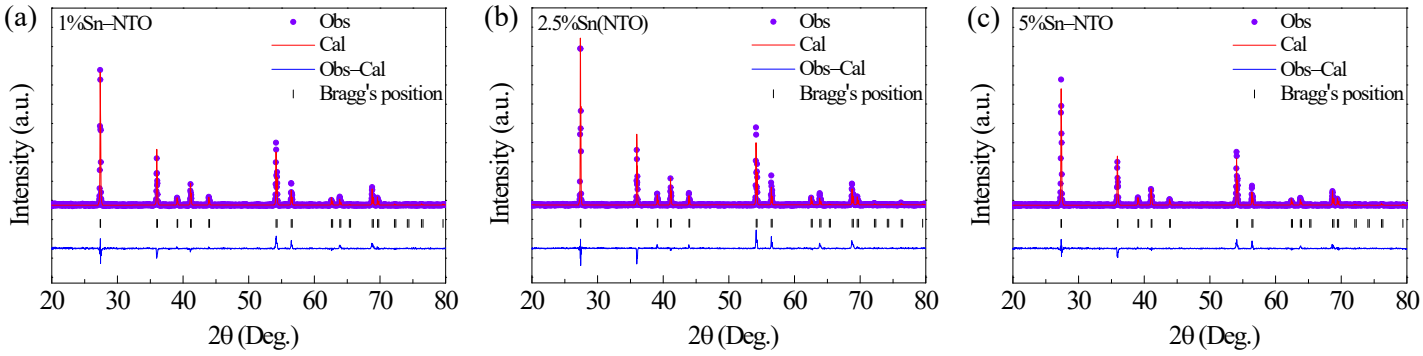

Fig. S2 Rietveld profile fitting for (a) 1%Sn–NTO, (b) 2.5%Sn–NTO, and (c) 5%Sn–NTO ceramics.

Fig. S2 illustrates the Rietveld refinement fitting for the 1%Sn–NTO, 2.5% Sn–NTO and 5% Sn–NTO ceramics, repectively, using X'pert High Score Plus program. A rutile TiO_2 phase was observed in all samples. Lattice parameters (*a* and *c*) and bond lengths (**A**–O and **A**–**A**, where **A=** Ta, Sn, Ti) were calculated and summarized in Table 1. These values increased with higher Sn^{4+} concentrations. The results were attributed to the effect of Nb^{5+} and Sn^{4+} radii, where $r_6(Nb^{4+})$ = 64.0 pm and $r_6(Sn^{4+})$ = 69.0 pm, which are larger than the Ti^{4+} host ions ($r_6(Ti^{4+})$ = 60.5 pm) by approximately 5.8% and 14.0%, respectively [2, 3]. The variance in dopant radii is was associated with the expansion of lattice parameters and bond lengths, influenced by the presence of Sn^{4+} ions. Importantly, the absence of a second phase in the 1–5%Sn–NTO ceramics indicated that both dopants completely replaced Ti^{4+} sites [2].

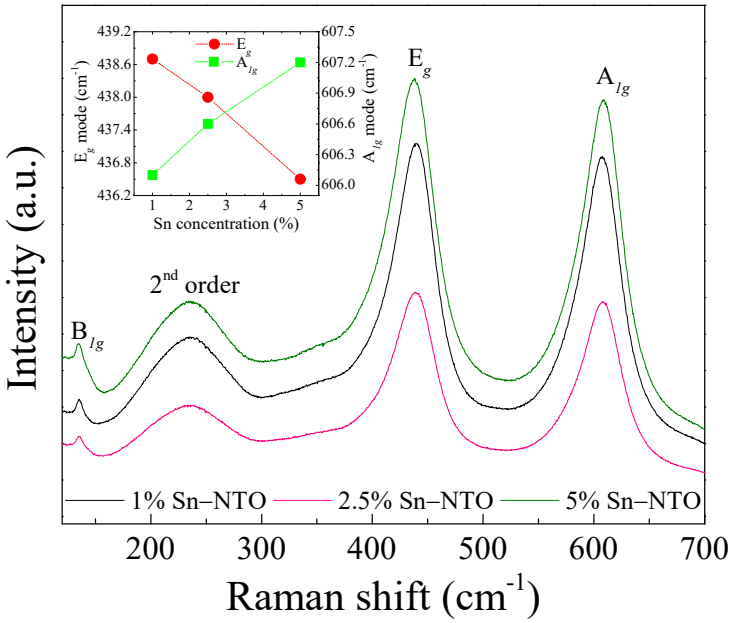

Fig. S3 Raman spectra of Sn–NTO ceramics sintered at 1200 °C for 3h. The inset shows Raman shift of E_g and A_{1g} modes of Sn–NTO ceramics as a function of Sn^{4+} concentrations.

Fig. S3 shows Raman peaks of rutile TiO_2 include B_{1g}, E_g and A_{1g} modes, as well as the multi–phonon peak of a second–order (2^{nd} order) effect for Sn–NTO ceramics [4, 5]. In the inset of Fig. S3, the Raman peaks of E_g were revealed to shift toward the low energy side in the range from 439 to 437 cm^{-1} with increasing Sn^{4+} concentrations. The result can be attributed to the lattice distortion and the movement of oxygen along c–axis [4]. In contrast, the A_{1g} mode exhibited a slight shift to higher frequency side from 601 to 607 cm^{-1} with increasing Sn^{4+} concentrations, as a result of the influence of the Ti–O stretch modes [6]. Both E_g and A_{1g} peak shift values were determined using the Lorentz model, as listed in Table 1.

Reference

[1] M. Zhong, J. Li, J. Shao, Y. Cao, K. Li, W. Zhao, An investigation into the enhanced permittivity properties of Zr co-doped $(Ga_{0.5}Nb_{0.5})_{0.03}Ti_{0.97O2}$ ceramics, Ceramics International, 45 (2019) 14983-14990.

[2] J. Fan, T. Yang, Z. Cao, Colossal permittivity and multiple effects in (Zn + Ta) codoped TiO_2 ceramics, Journal of Asian Ceramic Societies, 8 (2020) 1188-1196.

[3] J. Fan, Y. Chen, Z. Long, L. Tong, G. He, Z. Hu, Giant dielectric response and relaxation behavior in (Tm + Ta) co-doped TiO_2 ceramics, Phys Chem Chem Phys, 24 (2022) 4759-4768.

[4] G. Liu, H. Fan, J. Xu, Z. Liu, Y. Zhao, Colossal permittivity and impedance analysis of niobium and aluminum co-doped TiO_2 ceramics, RSC Advances, 6 (2016) 48708-48714.

[5] J. Fan, Z. Long, Z. Hu, High dielectric performance and multifarious polarizations in (Lu + Ta) co-doped TiO_2 ceramics, Journal of Asian Ceramic Societies, 9 (2021) 1255-1264.

[6] W. Tuichai, S. Danwittayakul, J. Manyam, N. Chanlek, M. Takesada, P. Thongbai, Giant dielectric properties of Ga^{3+}–Nb^{5+}Co-doped TiO_2 ceramics driven by the internal barrier layer capacitor effect, Materialia, 18 (2021) 101175.